Reports

High-Resolution Proton Nuclear Magnetic Resonance Analysis of Metastatic Cancer Cells

Abstract. *High-resolution proton nuclear magnetic resonance (NMR) studies of intact cancer cells revealed differences between cells with the capacity to metastasize and those that produce locally invasive tumors. The NMR resonances that characterize the metastatic cells were associated with an increased ratio of cholesterol to phospholipid and an increased amount of plasma membrane–bound cholesterol ester. High-resolution NMR spectroscopy could therefore be used to assess the metastatic potential of primary tumors.*

The ability of a cell to metastasize may be attributed in part to the characteristics of the cell membrane, in particular the cell surface components (*1*). However, cell surface characteristics are determined in part by the modulating effects of the plasma membrane lipids (*2*). In a study of the role of plasma membrane components in metastasis (*3*), the metastatic potential was transferred with the plasma membrane by fusing the shed plasma membrane vesicles of one cell line with another. The possibility was considered that membrane-bound proteins are the likely candidate for transfer of metastatic potential. We are considering the alternative possibility that the lipid molecules transferred during the fusion could be responsible for activating membrane-bound protein in the acceptor cell by altering the phase-transition properties of the membrane and, hence, the metastatic potential.

We now describe our study of the changes in the plasma membrane lipid associated with the metastatic process by means of chemical analysis of isolated enriched plasma membranes and high-resolution proton nuclear magnetic resonance (^{1}H NMR) spectroscopy. Proton NMR can be used to study the plasma membranes of intact viable lymphoblasts (*4, 5*), and we have applied this technology to the study of tumor cells with differing metastatic ability.

A rat mammary adenocarcinoma model developed for the study of cancer metastasis (*6*) was used to compare the membranes of the malignant and metastatic cell line 13762 and the malignant but nonmetastatic J clone (*6*). Approximately 6 weeks after subcutaneous injection of line 13762 cells (10^7) into the mammary line of a Fisher rat, tumors (~40 by 45 mm in size) develop and macroscopic spontaneous metastatic foci appear in the lungs. In contrast, J clone cells (10^8) produce a tumor of the same size after 7 weeks, but no metastatic foci are evident either macroscopically or microscopically.

In the 400 MHz ^{1}H NMR spectrum of line 13762 cells (Fig. 1A), the resonances are due to the fatty acyl chains of lipids within the bilayer of the plasma membrane (*4*), with the $-C{=}C-$, $N(CH_3)_3^+$, $-(CH_2)_n-$ and $-CH_3$ resonances at 5.2, 3.2, 1.2, and 0.9 parts per million (ppm), respectively. The unusually narrow resonances are thought to arise from small membrane domains that retain their integrity within the plasma membrane and tumble isotropically, producing narrow lines distinct from the remaining lipids in the membrane (*5*). These isotropically tumbling membrane domains, observed in both single cell suspensions and excised solid tumors, are not in diffusive contact with the remaining nuclei that give rise to the broad underlying resonances in the spectrum (*5*). Thus, in contrast to most known membrane systems where diffusion affects the relaxation of constituent molecules, measurement of the transverse relaxation parameter (T_2) is acceptable for some lipids in the plasma membranes of cancer cells.

The relatively narrow ^{1}H NMR resonances in the methylene region of the spectra of some cancer cells were resolved further into multiple components by Lorentzian-Gaussian deconvolution (Fig. 1B), allowing measurement of transverse relaxation for individual acyl-chain lipid components (*5*). At 400 MHz it was not possible to separate the lipid $-CH_3$ resonance from those arising from residual tissue culture medium.

Both metastatic line 13762 cells and nonmetastatic J clone cells gave four clearly resolved resonances under the broad methylene resonance (1.2 ppm). Application of the Meiboom-Gill modification of the Carr-Purcell (CPMG) pulse sequence (*7*) revealed different relaxation rates for these subcomponents, and further resolution enhancement was

Table 1. Transverse relaxation parameter (T_2) for the methylene resonance in line 13762 and J clone cells. Values for T_2 were calculated by a least-squares method. All values gave an r^2 greater than 0.98. Results are expressed as the mean ± standard error of the mean of three experiments.

Chemical shift (ppm)	T_2 (milliseconds)	
	13762 cells	J clone cells
Unmodified spectra		
1.2	21 ± 3	32 ± 6
	86 ± 16	154 ± 18
	772 ± 50	
Resolution-enhanced spectra		
1.22	19 ± 4	50 ± 14
	99 ± 27	136 ± 42
1.23	42 ± 12	63 ± 17
	167 ± 64	224 ± 44
1.25	28 ± 3	55 ± 13
	797 ± 106	117 ± 20
1.27	31 ± 4	38 ± 9
	162 ± 52	157 ± 36

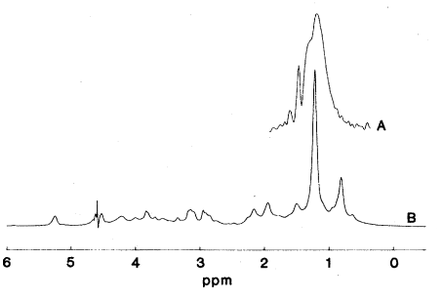

Fig. 1. The 400 MHz ^{1}H NMR spectra of the mammary adenocarcinoma metastatic cell line 13762. Cells (5×10^7) were suspended in 0.5 ml of phosphate buffered saline containing Ca^{2+} and Mg^{2+} in D_2O. Cells (5×10^6) were grown in RPMI 1640 medium supplemented with 10 percent fetal bovine serum at 37°C. Cells were maintained and studied in the logarithmic phase of growth; the doubling time was 24 to 26 hours. Data were recorded with the sample spinning at 37°C. The water peak was suppressed by gated irradiation (*5*). Sweep width, 4000 Hz; acquisition time, 1.64 seconds; 64 accumulations. (A) A line-broadening of 3 Hz was applied. (B) A Lorentz-Gaussian resolution enhancement performed as described (*15*), with $K = 11$ Hz, $g = 0.04$, and $a = 1.64$ seconds was applied to the free induction decay recorded for the same sample (K is the line-broadening function, g is the fraction of the free induction decay to be enhanced, and a is the acquisition time for the free induction decay. An expansion of the spectrum from 1.3 to 1.1 ppm is shown.

Table 2. Purity of membrane preparations of line 13762 and J clone cells. Plasma membranes were isolated from 2.5×10^8 cells (*15*). Purity was calculated by the specific activity of the marker in the membrane divided by that in the homogenate. The activities of acid phosphatase and lactate dehydrogenase suggest that the lysosomal and cytoplasmic contamination was reduced by the enrichment procedure. The absence of measurable succinate dehydrogenase activity confirms that there was no mitochondrial contamination. Activity of NADPH (reduced nicotinamide adenine dinucleotide phosphate)–cytochrome C reductase (the marker for endoplasmic reticulum) was higher than expected.

Enzyme marker	Purity		Reference
	13762 cells	J clone cells	
5′-Nucleotidase	3.1	4.1	(*16*)
Mg^{2+} adenosinetriphosphatase	2.7	2.5	(*17*)
Acid phosphatase	0.9	1.4	(*17*)
Lactic dehydrogenase	0.11	0.11	(*17*)
NADPH-cytochrome C reductase	1.6	1.8	(*18*)
Succinate dehydrogenase	None	None	(*19*)

Table 3. Lipid composition of enriched plasma membranes from line 13672 and J clone cells. Plasma membranes from 2.5×10^8 cells were resuspended and the lipid extracted (*20, 21*). Values and standard errors were determined from assays run in duplicate on three different extractions. The free cholesterol and total cholesterol contents of the total membrane lipid extract were determined by an enzymic fluorometric method (*22*). Cholesterol ester content was calculated by subtracting the free cholesterol from the total cholesterol content. Lipid phosphorus was determined colorimetrically on the total extracts as described (*23*). Triglyceride was determined colorimetrically (*24*) using the molecular weight of triolein (891). The mean molecular weight for phospholipid was taken as 750.

Cell line	Moiety (nanomoles per milligram of lipid)			Cholesterol: phospholipid ratio
	Triglyceride	Free cholesterol	Cholesterol ester	
13762	86 ± 9	278 ± 21	45 ± 7	0.40 ± 0.04
J clone	77 ± 6	236 ± 9	6 ± 6*	0.29 ± 0.03

*Mean ± standard error of the mean for two experiments.

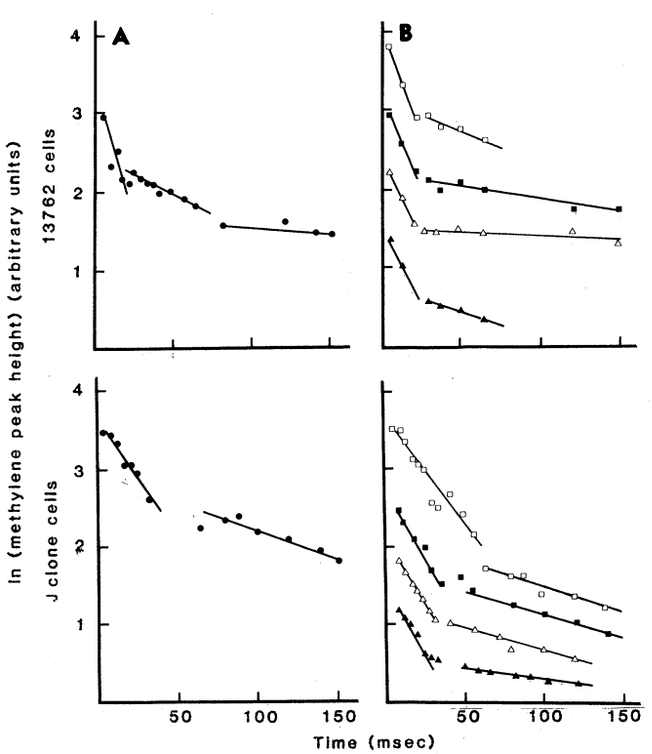

Fig. 2. The Meiboom-Gill modification of the Carr-Purcell pulse sequence (*7*) was applied to the mammary adenocarcinoma metastatic cell line 13762 and the nonmetastatic line J clone. The cell sample was prepared as described in the legend to Fig. 1, and the pulse sequence was excited as described (*5*). Thirty-two executed accumulations were recorded with the water resonance suppressed by gated irradiation (*5*). (A) Intensity of the methylene resonance plotted against the delay between the first pulse and the *n*th echo. These spectra had a line-broadening of 3 Hz. Only one methylene resonance was observable. (B) Similar to (A) but with a Lorentzian-Gaussian resolution enhancement ($K = -11$ Hz; $g = 0.04$; $a = 1.64$ seconds). Four resonances are observable at 1.22 ppm (□), 1.23 ppm (■), 1.25 ppm (△), and 1.27 ppm (▲).

achieved by varying the interpulse delay. Both single cell suspensions and solid tumors gave the profiles observed for the plot of the unmodified spectra in Fig. 2. The enhancement technique clearly resolved the resonances underlying the broad methylene resonance for most cell suspensions; however, the line width of resonances arising from a solid tumor can be much broader, and separation of the underlying resonance was sometimes difficult.

In the resolution-enhanced CPMG spectra of the metastatic line 13762 cells, four resonances at 1.22, 1.23, 1.25, and 1.27 ppm were resolved under the acyl chain resonance (1.2 ppm). Each of these four resonances showed two rates of decay (Fig. 2). In contrast, the unmodified broad $-CH_2-$ resonance showed three rates of decay, which were a composite of the three underlying peaks and were attributed to the resonance at 1.22 over the delay ranges 0 to 20 msec and 30 to 80 msec. The third and slowest rate was clearly due to the resonance at 1.25 ppm over the range 80 to 150 msec; this resonance clearly differentiated the cells with metastatic potential from the nonmetastatic variant (Fig. 2). A long T_2 has also been observed in two human cell lines with both low and intermediate metastatic phenotypes (*8, 9*).

The resolution-enhanced spectra of the nonmetastatic J clone cells also had four resonances at 1.22, 1.23, 1.25, and 1.27 ppm, but it was difficult to determine which, if any, of the resonances dominated the two rates observed in the unmodified $-CH_2-$ resonance (Fig. 2). However, the resonance at 1.25 ppm did not have the long T_2 observed for the equivalent resonance in the metastatic parent line (see Table 1).

In cell mixtures containing both the J clone and 13762 lines, as little as 20 percent line 13762 cells was detectable by ^1H NMR relaxation experiments. Mixing the two cell lines did however affect the spectral resolution, resulting in a greater scatter of points in the plot of peak height against delay between pulses. Despite this reduction in spectral resolution a multiphasic plot, indicating the presence of metastatic cells, was still clearly observable, and the points of inflection between the three different relaxation rates changed progressively with increasing numbers of metastatic cells. A similar reduction in spectral resolution recorded in other rat mammary adenocarcinoma cells with intermediate or low metastatic potential suggested that heterogeneity of the sample was responsible.

Solid tumors were grown along the mammary line of Fisher rats by injection of a suspension of cells. There was little observable difference between 400 MHz ^{1}H NMR spectra of a primary 13762 tumor and a J clone tumor, and it was also sometimes difficult to distinguish the four resonances under the $-CH_2-$ resonance in the spectra from tumor samples even after resolution-enhancement techniques were applied. However, when the CPMG pulse sequence was used the 13762 primary tumor gave the same three relaxation rates observed for the single cell suspension shown in Fig. 2. Similarly, the J clone tumor had only two relaxation rates that were comparable with those measured for the single cell suspension. The relaxation rates of secondary tumors excised from the lungs of the rats injected subcutaneously with line 13762 cells were compared with the primary tumors from the same animals and found not to differ.

A phenotypic drift of the J clone toward the metastatic parent line was observed twice in a solid tumor grown from cells that were injected subcutaneously into Fisher rats and were originally believed to lack metastatic potential. The results of CPMG experiments were characteristic of neither a line 13762 nor a J clone profile but of a composite of the two. There was no observable decrease in spectral resolution, suggesting that a high percentage of the cells had changed in a similar manner. The lungs of all tumor-bearing animals were sectioned and counted (*10*). The partially reverted J clone tumor (in a rat inoculated with 10^8 cells) showed a mean of nine colonies in each 5-μm section, each colony containing 100 to 125 cells. A nonreverted J clone tumor showed no metastases at all, whereas the line 13762 tumor (in a rat inoculated with 10^7 cells) showed the highest incidence of metastatic replacement, with 85 percent of the lung tissue involved.

Biochemical analysis of the plasma membranes of line 13762 and J clone cells was performed to determine which of the membrane components might be responsible for the differences in the ^{1}H NMR spectra of these cells and their related tumors. The plasma membranes from both line 13762 and J clone cells were enriched three- to fourfold by biochemical purification to remove any other membrane contaminants. The extent of the enrichment and purity was determined by markers for plasma membrane and constituents of the cells (Table 2). With the exception of lysosomal content, the enriched plasma membranes of both cell types were experimentally comparable in their purity.

There were unusually high concentrations of triglycerides in membranes of both the 13762 and J clone cell lines (Table 3). A significantly higher (~eightfold) amount of cholesterol ester in the metastatic line 13762 membrane fraction than in the J clone fraction was accompanied by a higher ratio of cholesterol to phospholipid (Table 3). Also, enriched plasma membranes from two J clone regressed cell lines in tissue culture contained 35 and 42 nmol of cholesterol ester per milligram of lipid, approximately the same amount as that in line 13762 cells (Table 3).

The presence of both triglycerides and cholesterol esters in a plasma membrane is unusual (*11*). The main source of contamination in this plasma membrane preparation was the endoplasmic reticulum, which is unlikely to explain the presence of the triglycerides. Cholesterol ester is known to be present within the endoplasmic reticulum, but its contamination was similar in the two cell lines. It is therefore unlikely that the significantly greater amount of cholesterol ester in the line 13762 cells was due to contamination from the endoplasmic reticulum or to lysosomes, which are more abundant in J clone cell membranes.

On the basis of these results, we conclude that ^{1}H NMR spectroscopic study of the unusual plasma membranes of cancer cells may provide insight into the metastatic ability of the cells. Although at this stage the identity of the resonance at 1.25 ppm is not clear, it is possible that the long T_2 in metastatic cells is related to the increased cholesterol ester content of their membranes. Moreover, triglycerides have been shown to exhibit properties similar to polar lipids in a bilayer (*12*), and we have also confirmed the presence of triglycerides in the plasma membrane of cultured leukemic lymphoblasts (*13*). In conjunction with the relatively small amount of free cholesterol, triglycerides could be responsible for the formation of the small membrane domains that give rise to the NMR signals. Although little is known about the effect of triglycerides in membranes, studies on lipoproteins have suggested that cholesterol esters change from the cholesteric to the smectic phase in the presence of triglycerides. Several studies have shown the fatty acid composition to influence the phase behavior of cholesterol esters (*14*). Thus, any increase in the amount of cholesterol ester or alteration in the type of acyl chain involved could change the phase transition of these small membrane domains. Changes in the phase-transition temperature of membranes can affect the activity of membrane-bound proteins and enzymes as well as the permeability and overall stability of the membrane. This is consistent with our preliminary observations that different phase-transition properties exist for lipids isolated from plasma membranes of line 13762 and J clone cells.

CAROLYN E. MOUNTFORD
LESLEY C. WRIGHT
KERRY T. HOLMES
WANDA B. MACKINNON
PATRICIA GREGORY
RICHARD M. FOX
Ludwig Institute for Cancer Research, Sydney Branch, University of Sydney, Sydney, N.S.W. 2006, Australia

References and Notes

1. J. A. Regato, *Cell Semin. Oncol.* **4**, 33 (1977).
2. S. Ladisch, B. Gillard, C. Wong, L. Ulsh, *Cancer Res.* **43**, 3808 (1983).
3. G. Poste and G. L. Nicolson, *Proc. Natl. Acad. Sci. U.S.A.* **399**, 403 (1980).
4. C. E. Mountford, G. Grossman, G. Reid, R. M. Fox, *Cancer Res.* **42**, 2270 (1982).
5. C. E. Mountford, W. B. Mackinnon, M. Bloom, E. Burnell, I. C. P. Smith, *J. Biochem. Biophys. Methods* **9**, 323 (1984).
6. I. A. Ramshaw, S. T. Carlsen, D. Hoon, R. C. Warrington, *Int. J. Cancer* **30**, 601 (1982).
7. S. Meiboom and D. Gill, *Rev. Sci. Instr.* **29**, 688 (1958).
8. A human colon carcinoma model developed for study of metastatic potential was provided by B. Sordat. NMR studies have confirmed that the resonance at 1.25 ppm in the metastatic variant has a T_2 of about 700 ± 150 msec, which is comparable to that measured for the rat mammary adenocarcinoma metastatic line. The nonmetastatic variant from this model did not show a T_2 value of above 150 msec for the same resonance (*13*).
9. Human ovarian lines of varying degrees of metastatic potential (supplied by C. van Haaften-Day) again showed the presence of a long T_2 relaxation parameter for the resonance at 1.25 ppm (*13*).
10. B. Boeryd, T. Ganeluis, P. Lundin, J. Mellgren, *Int. J. Cancer* **1**, 497 (1966).
11. C. Green, in *International Reviews of Biochemistry*, T. W. Goodwin, Ed. (University Park Press, Baltimore, 1977), vol. 14, part 2.
12. H. Gorrissen, A. P. Tulloch, R. J. Cushley, *Chem. Phys. Lipids* **31**, 245 (1982).
13. C. E. Mountford *et al.*, unpublished data.
14. D. Armitage, R. J. Decklebaum, G. G. Shipley, D. M. Small, *Mol. Cryst. Liq. Cryst.* **42**, 203 (1977); D. M. Small, in *Surface Chemistry of Biological Systems*, M. Blank, Ed. (Plenum, New York, 1970), p. 55; G. S. Ginburg and D. M. Small, *Biochim. Biophys. Acta* **664**, 98 (1981); R. J. Deckelbaum, G. G. Shipley, D. M. Small, *J. Biol. Chem.* **252**, 744 (1977); A. R. Tall, D. M. Small, D. Atkinson, L. L. Rudie, *J. Clin. Invest.* **62**, 1354 (1978).
15. Washed cells were resuspended in 4 volumes of cavitation buffer [100 m*M* tris-HCl (*p*H 7.4), 10 m*M* $MgCl_2$, 10 percent (weight by volume) sucrose, and 1 m*M* phenylmethylsulfonyl fluoride evaporated from acetone solution]. The cells were disrupted in a Parr pressure bomb under 800 pounds per square inch for 15 minutes. The suspension was centrifuged for 5 minutes at 1000*g*, and the pellet was again disrupted for 15 minutes at 800 pounds per square inch. The bulked supernatants were centrifuged at 130,000*g* for 90 minutes to obtain the membrane pellet.
16. R. M. Fox, E. M. Tripp, S. K. Piddington, M. H. N. Tattersall, *Cancer Res.* **40**, 3383 (1980).
17. B. N. Ames, *Methods Enzymol.* **8**, 115 (1965); Boheringer Mannheim GmbH diagnostica lactate dehydrogenase test kit (catalogue No. 124907).
18. G. L. Sottocasa, B. Kuylenstierna, L. Emster,

A. Bergstrand, *J. Cell. Biol.* **32**, 415 (1967).
19. H. Maeno, E. M. Johnson, P. Greengard, *J. Biol. Chem.* **246**, 134 (1971).
20. E. L. Gottfried, *J. Lipid Res.* **8**, 321 (1967).
21. J. P. Williams and P. A. Merrilees, *Lipids* **5**, 367 (1970).
22. J. G. Heider and R. L. Boyett, *J. Lipid Res.* **19**, 514 (1978).
23. C. G. Duck-Chong, *Lipids* **14**, 492 (1979).
24. *Sigma Technical Bulletin* **405**, 1 (1977).
25. We thank I. Ramshaw, B. Sordat, and C. Van Haaften-Day for supplying the cell lines and their many helpful discussions and M. H. N. Tattersall for continued support.

4 June 1984; accepted 29 October 1984

Contribution of Small Glaciers to Global Sea Level

Abstract. *Observed long-term changes in glacier volume and hydrometeorological mass balance models yield data on the transfer of water from glaciers, excluding those in Greenland and Antarctica, to the oceans. The average observed volume change for the period 1900 to 1961 is scaled to a global average by use of the seasonal amplitude of the mass balance. These data are used to calibrate the models to estimate the changing contribution of glaciers to sea level for the period 1884 to 1975. Although the error band is large, these glaciers appear to account for a third to half of observed rise in sea level, approximately that fraction not explained by thermal expansion of the ocean.*

Sea level appears to have risen 10 to 15 cm in the last 100 years, and part of this rise may be due to thermal expansion of the oceans (*1–3*). The remainder has generally been attributed to melting of polar ice. However, studies of the current mass balance of the Antarctic ice sheet, which makes up about 85 percent of the total glacier ice area on the earth, suggest that a negative mass balance is not likely and that this ice sheet may be subtracting water from the world ocean (*4, 5*). Recent estimates of the mass balance of the Greenland ice sheet (12 percent of the world's glacier ice area) suggest that it is close to balance (*4, 6*). If the remaining 3 percent of the earth's glacier ice area accounts for the unexplained rise in sea level, might a further addition to sea level be expected from these small glaciers as the climate warms because of the increased concentration of CO_2 and other "greenhouse" gases?

Because data on glacier measurements are sparse, a 61-year average change in glacier mass was calculated from the meager volume change data and scaled to a global estimate by considering the intensity of the seasonal mass balance fluxes. This result, together with data from the few long-term balance models, is used to estimate the annual contribution of water to the ocean between 1884 and 1975. The Antarctic and Greenland ice sheets and the smaller glaciers near them are not considered.

Glacier observations that are available include measurements of advance or retreat, mass balance histories derived from snow pits and ice cores, volume changes, direct measurements of annual and seasonal mass balances, and mass balance sequences extended by use of numerical models. Most of the data and the longest records are of the first two types and are virtually impossible to use to infer long-term changes in ice mass. Advance-retreat data do not provide volume change information and can be misleading in sign; a glacier can increase in volume and retreat at the same time. Stratigraphic measurements of balances in pits and cores are taken at single locations in the accumulation area, which is insufficient to infer the mass change of the entire glacier. Direct measurements of mass balance, made on the glacier surface, provide short-term results; the oldest series was started in 1945, and only 37 glaciers were being so measured before the beginning of the International Hydrological Decade in 1965. Thus, this analysis is based mainly on long-term volume change data and the results of numerical mass balance models.

The mass balance (b) of a glacier is the difference in water equivalent between input (accumulation) and outgo (ablation) at the surface, averaged over the area of the glacier (G), which is a function of time (t) (*7*)

$$\Delta V = \frac{1}{\rho} \int_{t_0}^{t_1} b(t)G(t)dt \qquad (1)$$

where ΔV is the long-term volume change, and ρ is the specific gravity of the glacier, which is assumed not to change. Because sufficient data are generally not available, I use the approximation

$$\bar{b} = \frac{\rho \Delta V}{(t_1 - t_0)\bar{G}} \qquad (2)$$

where $\bar{G}$ is the average area of the glacier during the interval $t_0 < t < t_1$, to estimate the long-term mean balance $\bar{b}$ (*8*).

Simple statistical models have been used to develop long-term balance sequences from a short sequence of measured balances combined with long-term records at meteorological and hydrological stations. These hydrometeorological (HM) models generally relate accumulation on the glacier to winter precipitation, ablation to summer air temperature, and the net balance to the difference between accumulation and ablation; runoff may be used to calibrate input and output (*9*). These statistical relations, however, may not be stationary over long periods of time, and as a result the long-term mean balance may be seriously in error (*10*). In very few cases, the estimated mean balances have been calibrated or checked against known volume changes; these calibrated HM models provide results that can be used with confidence (*11*).

Data on glacier balance and volume change for periods exceeding 50 years for 25 glaciers (Table 1) were taken from reports of the Permanent Service on the Fluctuations of Glaciers (*12*) and other sources (*13*). The mean period of record for those glaciers is from 1900.5 to 1961.7; HM sequences for the interval 1900 to 1961 were used to make the data set more homogenous. The unweighted average of the 25 mean balances is -0.40 m/year in water equivalent (standard deviation, 0.25); the mean of the 13 regional averages is -0.34 ± 0.20 m/year; and the mean of the regional averages weighted by quality of the data (*14*) is -0.38 ± 0.20 m/year.

The 25 glaciers with long-term data occur in only 13 regions (Table 1) and constitute a biased sample of the world's glaciers: all but one are between 38° and 69°N latitude; none is at low latitudes or in the Southern Hemisphere. Thus a method is needed to relate these results to an estimate of the mass balance of the earth's entire cover of glaciers.

I suggest that the magnitude of the long-term balance may be related to the magnitude of the seasonal mass fluxes (accumulation and ablation) and that this may be used as a scaling factor to derive global estimates. The annual mass balance amplitude is defined as

$$a = (b_w - b_s)/2 \qquad (3)$$

where b_w is the winter balance and b_s (normally negative) is the summer balance (*7, 15*). Winter and summer balances are used instead of annual accumulation and ablation, respectively, which are rarely measured. Values of the annual amplitude can be calculated for most of the world's glacier areas from data reported since 1965 (*12*) and can be estimated for other areas because annual amplitude is primarily a function of the climatological regime. The annual amplitude is highest at temperate to subarctic (and subantarctic) latitudes, lowest near the poles, and also decreases with increasing continentality (Table 1). Gla-